# Ultrasonic Assisted Adsorption of Crystal Violet (CV) Dye onto Synthesized CM-β-CD-Fe₃O₄NPs: Experimental Design Methodology

Ali Omani Ziarati[1], Gholamhossein Vatankhah[2]*

[1]Department of Chemical Engineering, Dashtestan Branch, Islamic Azad University, Dashtestan, Iran
[2*]Department of Chemical Engineering, Bushehr Branch, Islamic Azad University, Bushehr, Iran

Corresponding author E-mail: gh.vatankhah@iau.ac.ir

## ABSTRACT

In this study the applicability of the synthesized CM-β-CD-Fe₃O₄NPs as a novel adsorbent was investigated for eliminating Crystal Violet (CV) dye from aqueous media. This work focuses on the development of an effective methodology to obtain the optimum removal conditions assisted by ultrasonic to maximize the removal of CV dye onto CM-β-CD-Fe₃O₄NPs in an aqueous solution using response surface methodology (RSM). This novel adsorbent was characterized by different techniques such as FT-IR, XRD, and SEM. The influences of variables such as initial concentration of CV dye ($X_1$), pH ($X_2$), adsorbent dosage ($X_3$), and sonication time ($X_4$) were investigated by central composite design (CCD) under response surface methodology. The process was empirically modeled to reveal the significant variables and their possible interactions. The optimization conditions were set as: 10.0 mgL⁻¹, 6.0, 5.0 min, and 0.025 g, for ultrasound time, pH, adsorbent mass, CV dye concentration, respectively. Finally, it was shown that the removal of CV dye by adsorbent was at pH=6.0. This issue that the sorption of CV dye conforms to the pseudo-second-order kinetic equation and the Langmuir isotherm explains equilibrium data was clearly proven. The maximum monolayer capacity ($q_{max}$) was found to be 100.0 mg g⁻¹ for CV dye at optimum conditions. The exothermicity of the process was proven by the negative value of ($\Delta G^o$, $\Delta H^o$, and $\Delta S^o$) which showed the affinity of synthesized CM-β-CD-Fe₃O₄NPs for CV dye deletion.

**Keywords:** Adsorption, Crystal Violet (CV) Dye, CM-β-CD-Fe₃O₄NPs, Central Composite Design (CCD), Response Surface Methodology (RSM).

## 1. INTRODUCTION

The severity of water pollution due to human economic development is increasing worldwide. Textile industries consume huge quantities of water and generate an enormous amount of impurities including dyes, detergents, additives, suspended solids, aldehydes, heavy metals, non-biodegradable matter,

and insoluble substances [1, 2]. According to recent reports, more than one million dyes are commercially available with an annual production of over $7 \times 10^5$ tons. The textile industry worldwide consumes approximately $1 \times 10^4$ tons of dyes annually and discharges nearly 100 tons/year of dyes into wastewater [3]. Wastewaters of industries like textile, paper, rubber, plastic, leather, cosmetic, food, and drug industries contain dyes and pigments which are hazardous and can cause allergic dermatitis, skin irritation, cancer, and mutation in living organisms [4]. The importance of the potential pollution of dyes and their intermediates has been incited with the toxic nature of many dyes, different mutagenic effects, skin diseases, and skin irritation and allergies. Moreover, they are dangerous because their microbial degradation compounds, such as Benzedrine or other aromatic compounds have a carcinogenic effect [5]. Crystal violet (CV) is a cationic dye that can easily interact with negatively charged cells membrane surfaces, enter into cells, and can concentrate in the cytoplasm [6]. CV belongs to the triphenylmethane group, which is widely applied in coloring paper, temporary hair colorant, and dyeing cotton and wool. CV may harm the body via inhalation, ingestion, and skin contact. It has also been found to cause cancer and severe eye irritation to human beings [7, 8]. Adsorption is one of the best and simple techniques for the removal of toxic and noxious impurities in comparison to other conventional protocols such as flocculation, membrane filtration, advanced oxidation, ozonation, photocatalytic degradation, and biodegradation [9, 10]. These traditional methods have inherent limitations, such as the complex and uneconomical nature of the technology, and thus it is necessary to seek efficient and simple dye wastewater treatment methods [11]. Iron oxide

nanoparticles are widely used for metal remediation due to their low toxicity and easy separation from water media [12], in addition, where the nanoparticle (NP) is composed of magnetite, a facile magnetic separation of NPs, along with associated contaminants, can be performed. However, bare magnetite nanoparticles rapidly aggregate in aqueous systems and are highly susceptible to transformations under many environmental conditions [13, 14]. Among these methods, nanomaterial's based adsorbents are highly recommended for dyes pollutants removal [15]. The efficient applicability of an adsorption process mainly depends on the physical and chemical characteristics of the adsorbent, which is expected to have high adsorption capacity and to be recoverable and available at an economical cost. Currently, various potential adsorbents have been implemented for the removal of specific organics from water samples. In this regard, magnetic nanoparticles (MNPs) have been studied extensively as novel adsorbents with large surface areas, high adsorption capacity, and small diffusion resistance. For instance, they have been used for the separation of chemical species such as environmental pollutants, metals, dyes, and gases [16]. Cyclodextrins (CD) are natural nanoparticle that they are obtained by enzymatic digestion of starch. The α-, β- and γ- cyclodextrins contain respectively 6, 7, and 8 glucopyranose units, with primary and secondary hydroxyl groups located on the narrow and wider rims of a truncated cone shape structure [17]. The steric arrangement of glucose units in the CD molecule brings in the shape of a hollow truncated cone with a hydrophilic external surface and a hydrophobic internal cavity, which permits CDs to form inclusion complexes with different guest molecules [18]. The principal advantages of natural CDs as drug carriers are: (1) the

availability of CDs of different cavity sizes, (2) a well-defined chemical structure, yielding many potential sites for chemical modification [19]. In recent years, researchers have made the ability of cyclodextrin nanocomposite due to the structural, chemical, and biological stability of this nanocomposite to be a very good choice as a solid-phase extraction adsorbent for water treatment applications and by placing magnetite nanoparticles ($Fe_3O_4$) inside of CD, making it with a significant magnetic property that has many applications, especially as an effective adsorbent [20].

In the present work, CM-β-CD-$Fe_3O_4$NPs as a novel adsorbent was simply synthesized and subsequently characterized by scanning electron microscopy (SEM), Fourier transforms infrared spectroscopy (FTIR), and X-ray diffraction (XRD) analysis. In the process of CV dye deletion, the effects of important variables like contact time, pH of solution, adsorbent dosage, and CV dye concentration as well as the dye deletion percentage as a response were investigated and optimized. Via studying the experimental conditions of pH of the solution, contact time, initial CV dye concentration, adsorbent dosage, and the dye removal percentage, were investigated and optimized by central composite design (CCD) under response surface methodology (RSM). It was shown that the adsorption of CV dye follows the pseudo-second-order rate equation. The Langmuir model was found to be applied for the equilibrium data explanation. It was shown through the study of Kinetic models (both pseudo-first-order, pseudo-second-order diffusion models) that the kinetic of adsorption process is controlled by the pseudo-second-order model. The effectuality of CM-β-CD-$Fe_3O_4$NPs in deleting CV dye from wastewater was proven.
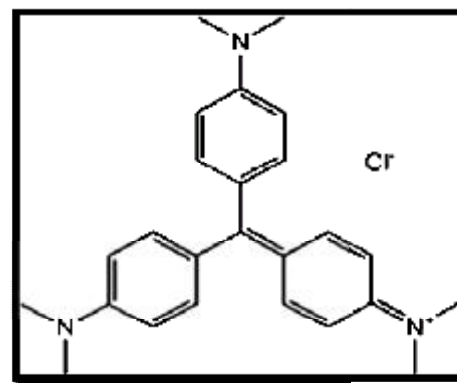


**Fig. 1.** The formula structure of Crystal violet dye.

## 2. EXPERIMENTAL
### 2.1. Materials and Reagents
CV dye (with formula structure shown in Fig. 1), Cyclodextrin CM-β-CD (99.0%), Ammonium hydroxide (98.0%), Iron (III) Chloride Hexahydrate (99.0%), and Iron (II) Chloride tetrahydrate (98.0%). Sodium hydroxide (98.0%), hydrochloric acid (37.0%), nitric acid (69.0%). They were supplied from Merck (Darmstadt, Germany). All used chemicals were of reagent grade and utilized without further purification. For the pH adjustment, hydrochloric acid ($HCl_{aq}$) and sodium hydroxide ($NaOH_{aq}$) were applied.

### 2.2. Instrumentation
The applied instruments were as follow: UV–Vis spectrophotometer (Model V-530, Jusco, Japan) at room temperature. Fourier transform infrared (FT-IR) spectra were registered on a PerkinElmer (FT-IR spectrum BX, Germany). SEM (Scanning electron microscopy: KYKY-EM 3200, Hitachi Firm, China) under an acceleration voltage of 26 kV was used to study the morphology of samples. An ultrasonic bath with a heating system (Tecno-GAZ SPA Ultrasonic System, Italy) at 60 Hz of frequency and 130W of power was used for the ultrasound-assisted adsorption procedure. For the measurement of pH, the pH/Ion meter (model-728, Metrohm Firm,

Switzerland) was employed. Laboratory glass wares were put overnight in 10% nitric acid solution. To set the temperature, A NBE ultra thermostat (VEB Prufgerate – Werk Medingen, Germany) was utilized. The pore structure parameters of materials such as $N_2$ adsorption-desorption isothermal curve were determined by micromeritics ASAP2010M adsorption analyzer. The sample was dropped onto the slide for conducting layer treatment, at 77 K liquid nitrogen temperature and the operating voltage was 20 kV. The specific surface areas of the samples were calculated using the Brunauer-Emmett-Teller (BET) method and the pore volumes and diameters were calculated by the Barret–Joyner–Halenda (BJH) method [21].

## 2.3. Preparation of CM-*β*-CD-Fe₃O₄NPs
Initially, a mixture of β-CD (2 g) and sodium hydroxide (1.86 g) in distilled water (7.5 ml) was treated with a 16.3% monochloroacetic acid solution (5.5 ml), precipitated with methanol, and dried at 50 °C under vacuum to give the CM-β-CD. CM-β-CD-Fe₃O₄NPs was briefly fabricated by 0.86 g of $FeCl_2 \cdot 4H_2O$, 2.35 g $FeCl_3 \cdot 6H_2O$ (molar ratio of $Fe^{2+}$: $Fe^{3+}$ = 1:2) and 1.5 g CM-β-CD were dissolved in 40 ml of deoxygenated water with vigorous stirring at a speed of 500 rpm. 40 ml of $NH_4OH$ (25%) was added slowly after the solution was heated to 90 °C. The reaction was continued for 1 h at 80°C under constant stirring and nitrogen environment. The synthesis of CM-β-CD-Fe₃O₄NPs was done under nitrogen flow for removing oxygen from the experiment medium. Indeed the $N_2$ (g) bubbling through the mixture, protects $Fe_3O_4$ against critical oxidation. The resulting nanoparticles were then washed with deionized water a few times to remove any unreacted chemicals and dried in a vacuum oven. The synthesis method of the

adsorbent samples is shown schematically in Fig. 2. Finally, the CM-β-CD-Fe₃O₄NPs adsorbent was treated from a leaf medlar in equal weight ratio, and then it was characterized by BET, XRD, FT-IR, and SEM analysis [19, 20].

$$FeCl_2.4H_2O + 2FeCl_3.6H_2O + 8NH_4OH = Fe_3O_4(s) + 8NH_4Cl + 20\ H_2O$$
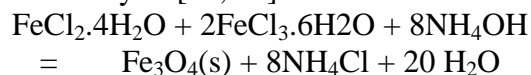
## 2.4. Adsorption experiments
According to experimental runs in the CCD, the pH of various solutions with different concentrations of CV dye was adjusted using concentrated HCl and/or NaOH into a 50 mL Erlenmeyer flask while mixed thoroughly with specific amounts of adsorbent. The experiments were performed at room temperature during predetermined sonication time in an ultrasonic. At the end of the adsorption process, the sample solution was immediately centrifuged and the supernatant containing residual was analyzed by UV-Vis spectroscopy. The removal percentage of CV dye (R %) at a given time and the amount of CV dye adsorbed after reaching the equilibrium ($q_e$ (mg g$^{-1}$)) was calculated from the following equations:

$$R\% = \frac{C_{oi} - C_{ei}}{C_{oi}} \times 100 \qquad (1)$$

$$q_i = \frac{V\ (C_{oi} - C_{ei})}{M} \times 100 \qquad (2)$$

$C_o (mgL^{-1})$ in the formula refers to the initial dye concentration and $C_e (mgL^{-1})$ represents the equilibrium dye concentration in an aqueous solution. V (L) shows the solution volume and W (g) signifies the adsorbent mass [22].

## 2.5. Ultrasound-assisted method
The removal of CV was examined using the ultrasound-assisted method to adsorption combined with CM-β-CD-Fe₃O₄NPs. The sonochemical adsorption
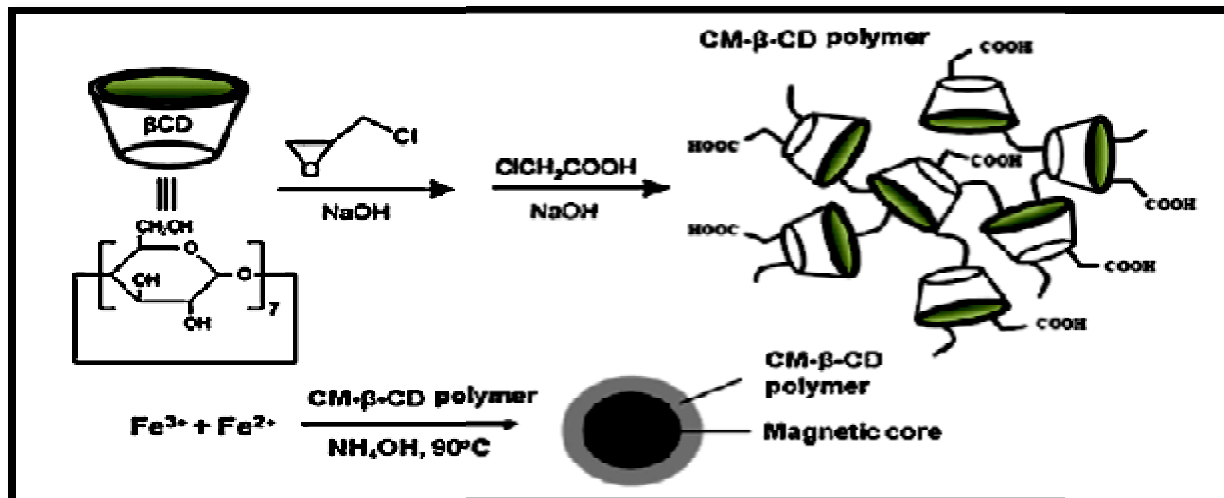
**Fig. 2.** Schematic representation of the synthesis of CM-β-CD-Fe$_3$O$_4$NPs.

experiment was carried out in a batch mode as follows: specified amounts of CV dye solution (50 mL) at the known concentration (10.0 mg L$^{-1}$ for CV concentration) and pH 6.0 with a known amount of adsorbent (0.03 g) were loaded into the flask and maintained the desired sonication time (4 min) at the 25$^o$C. The CV dye concentration in the solution was measured using a double beam UV–Vis spectrophotometer set at wavelengths 620 nm for CV dye (Fig. 3) [22].

**2.6. Central composite design (CCD)**
CCD is a method to reduce the number of experiments and cost, and to investigate the effects of parameters by designing experimental runs was applied for modeling and the optimization of effects of CV dye concentration ($X_1$), PH ($X_2$), amount of adsorbent ($X_3$) and contact time ($X_4$) on the ultrasonic-assisted adsorption of CV dye onto CM-β-CD-Fe$_3$O$_4$NPs [10, 23]. Four independent variables were set at five levels at which the R% of CV as a response was determined and shown in Tables 1 and 2. Analysis of variance (ANOVA) was studied to evaluate the significance and adequacy of the developed model by assessing the lack of fit, regression coefficient ($R^2$), and the Fisher test value (F-value), continuously, the mathematical relationship between the four independent parameters were obtained by a second-order polynomial response equation [24].

**Table 1.**Experimental factors, levels and matrix of CCD.

| Factors | levels | | | Star point$\alpha$ = 2.0 | |
|---|---|---|---|---|---|
| | Low (-1) | Central (0) | High(+1) | -$\alpha$ | +$\alpha$ |
| ($X_1$) CV dye Concentration (mg L$^{-1}$) | 10.0 | 15.0 | 20.0 | 5.0 | 25.0 |
| ($X_2$) pH | 5.0 | 6.0 | 7.0 | 4.0 | 8.0 |
| ($X_3$) Adsorbent mass (g) | 0.0150 | 0.0225 | 0.0350 | 0.0050 | 0.0450 |
| ($X_4$) Sonication time (min) | 3.0 | 4.0 | 5.0 | 2.0 | 6.0 |
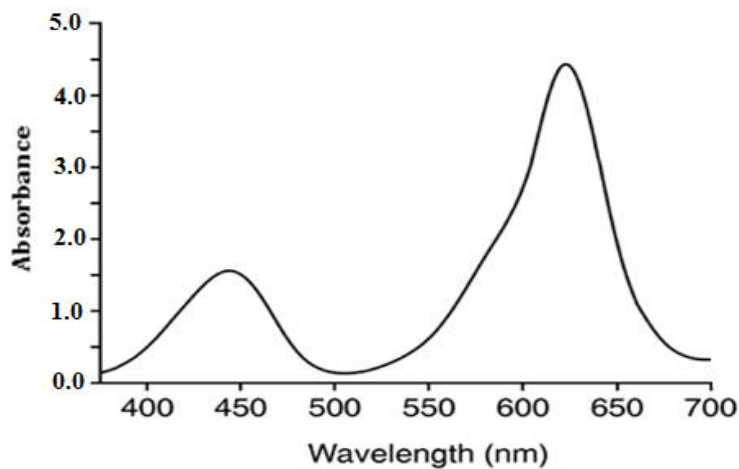
**Fig. 3.** Adsorption spectra of CV onto CM-β-CD-Fe$_3$O$_4$NPs sorbent in solution.

**Table 2.** The design matrix and the response

| Run | $X_1$ | $X_2$ | $X_3$ | $X_4$ | $\%R_{CV}$ |
|-----|-------|-------|-------|-------|------------|
| 1 | 10 | 7 | 0.035 | 5 | 98.00 |
| 2 | 15 | 4 | 0.025 | 4 | 95.00 |
| 3 | 20 | 7 | 0.035 | 6 | 97.90 |
| 4 | 25 | 6 | 0.025 | 4 | 98.00 |
| 5 | 15 | 6 | 0.025 | 4 | 94.45 |
| 6 | 10 | 7 | 0.015 | 2 | 88.00 |
| 7 | 10 | 7 | 0.035 | 6 | 100.00 |
| 8 | 15 | 8 | 0.025 | 4 | 97.50 |
| 9 | 15 | 6 | 0.025 | 4 | 95.00 |
| 10 | 15 | 6 | 0.025 | 4 | 94.70 |
| 11 | 20 | 7 | 0.015 | 6 | 95.00 |
| 12 | 10 | 5 | 0.035 | 2 | 100.00 |
| 13 | 15 | 6 | 0.025 | 4 | 95.00 |
| 14 | 15 | 6 | 0.025 | 4 | 97.00 |
| 15 | 10 | 5 | 0.035 | 6 | 100.00 |
| 16 | 15 | 6 | 0.025 | 4 | 95.00 |
| 17 | 20 | 5 | 0.015 | 6 | 73.00 |
| 18 | 15 | 6 | 0.005 | 4 | 70.00 |
| 19 | 20 | 5 | 0.015 | 2 | 80.00 |
| 20 | 20 | 7 | 0.035 | 2 | 99.69 |
| 21 | 10 | 5 | 0.015 | 2 | 88.50 |
| 22 | 20 | 5 | 0.035 | 2 | 100.00 |
| 23 | 15 | 6 | 0.025 | 4 | 95.00 |
| 24 | 15 | 6 | 0.045 | 4 | 100.00 |
| 25 | 15 | 6 | 0.025 | 8 | 99.48 |
| 26 | 10 | 5 | 0.015 | 6 | 99.33 |
| 27 | 5 | 6 | 0.025 | 4 | 100.00 |
| 28 | 10 | 7 | 0.015 | 6 | 100.00 |
| 29 | 15 | 6 | 0.025 | 7 | 100.00 |
| 30 | 10 | 5 | 0.035 | 6 | 100.00 |

## 2.7. Desirability function

Desirability function (DF) creates a function for each individual response leading to the final output of the global function (D), the maximum value of which supports the achievement of optimum value. The principle and application of the desirability function for the best prediction of the real behavior of the adsorption system were pointed out previously [25]. The desirability profiles indicate the predicted levels of variables, which produce the most desirable responses.

## 3. RESULTS AND DISCUSSION
### 3.1. Characterization of adsorbent
### 3.1.1. BET analysis of CM-*β*-CD-Fe₃O₄NPs

The porosity and chemical reactivity of functional groups at the surface control the adsorption capacity of CM-β-CD-Fe₃O₄NPs. The textural characteristics of the adsorbent samples were specified by $N_2$ adsorption/desorption (Fig. 4). The specific surface area, pore-volume, and pore diameter of the adsorbents were calculated using the BET and BJH method, respectively, and results are summarized in Table 3. These results illustrate that the synthesized adsorbents with higher surface area and pore volume, have high quality.

### 3.1.2. FTIR analysis

As demonstrated in Fig. 5, the FTIR spectrum of CM-β-CD-Fe₃O₄NPs presented clear broad signals at ≤900 in Fe–O, The absorption band at 876.3,

777.3, and 586.0 $cm^{-1}$ is due to the Fe–O bending in the molecules adsorbed into the surface 1445-1628 $cm^{-1}$ which can be regarded as being caused by C–H adsorption band 2368.23 $cm^{-1}$ from CM-β-CD-Fe₃O₄NPs, and the one at 1628.0 $cm^{-1}$ can be ascribed to C=O bonds [18].

The broad peaks at 1031.0 $cm^{-1}$ could be assigned to C–O stretching from phenolic, alcoholic, etheric groups and the broad peaks at 1155.0 $cm^{-1}$ to C–C bonds. The novel emerging signal at 2931.0 $cm^{-1}$ references C–H stretching and the novel emerging signal at 3567 $cm^{-1}$ is attributed to – OH stretching [19, 26].

### 3.1.3. XRD analysis

X-ray diffraction (XRD) analysis was performed and the results are presented in Fig. 5. Considering the fact that cellulose is the main component of CM-β-CD and according to the XRD result in Fig. 6, the peak at 2θ around 22º is evidence of cellulose. The synthetic Fe₃O₄NPs are crystalline in nature, as verified by the XRD pattern. As it can be observed in the XRD results of the CM-β-CD-Fe₃O₄NPs (Fig. 6), the diffraction peaks at 2θ= 38.21°, 44.18°, 64.52°, and 78.12° were assigned to the Fe₃O₄NPs [27]. Obviously, the perfect crystalline nature of the material was proven after functionalizing with CM-β-CD-Fe₃O₄NPs however the great intensity of the signal at 38.21 (311) confirmed that there has been a slight amount of material in the amorphous state.

**Table 3.** Textural properties of the CM-β-CD and CM-β-CD-Fe₃O₄NPs.

| Characterization | | Samples | |
|---|---|---|---|
| | | CM-β-CD | CM-β-CD-Fe₃O₄NPs |
| BJH desorption summary | Surface area (m²/g) | 65.95 | 65.71 |
| | Pore volume (m³/g) | 0.384 | 0.381 |
| | Pore diameter (Å) | 98.52 | 98.21 |
| BJH adsorption summary | Surface area (m²/g) | 88.97 | 88.68 |
| | Pore volume (m³/g) | 0.431 | 0.428 |
| | Pore diameter (Å) | 56.38 | 56.23 |
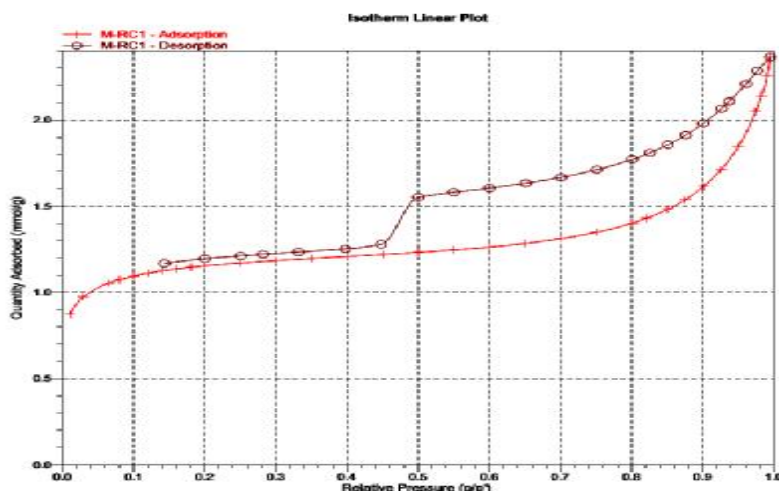
**Fig. 4.** N$_2$ adsorption–desorption isotherms of CM-β-CD-Fe$_3$O$_4$NPs.

The perfect synthesis of CM-β-CD-Fe$_3$O$_4$NPs is obvious through looking at the XRD pattern.

### 3.1.4. Surface morphology

The morphological properties of the investigated samples by SEM are exhibited in Fig. 7. As demonstrated in Fig. 7, the evenness, homogeneity, orderliness, and approximate uniformity of CM-β-CD-Fe$_3$O$_4$NPs (even in size distribution) was observed. After surface modification, CM-β-CD-Fe$_3$O$_4$NPs came to be uneven, bigger, and agglomerate. It has been seen

that the particles were mostly spherical with various size distributions. The particle size was also calculated using the Deba Schaer equation of 14-25 nm very close to those determined by XRD analysis [28].

### 3.2. Modeling the process and statistical analysis

Central composite design (CCD) under RSM was applied to design a systematic series of experiments (30 runs) in five levels. RSM makes it possible to nonlinearly model the experimental data [29, 30].
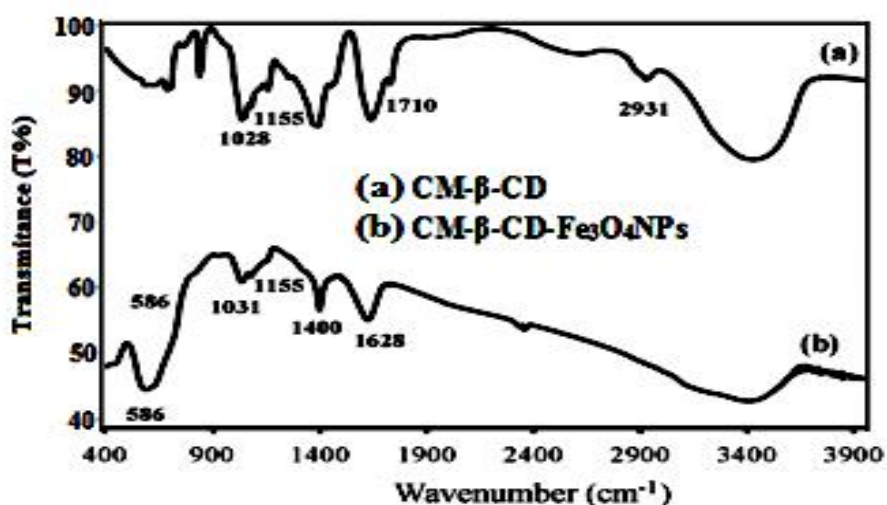


**Fig. 5.** FT-IR transmittance spectrum of the prepared CM-β-CD-Fe$_3$O$_4$NPs.
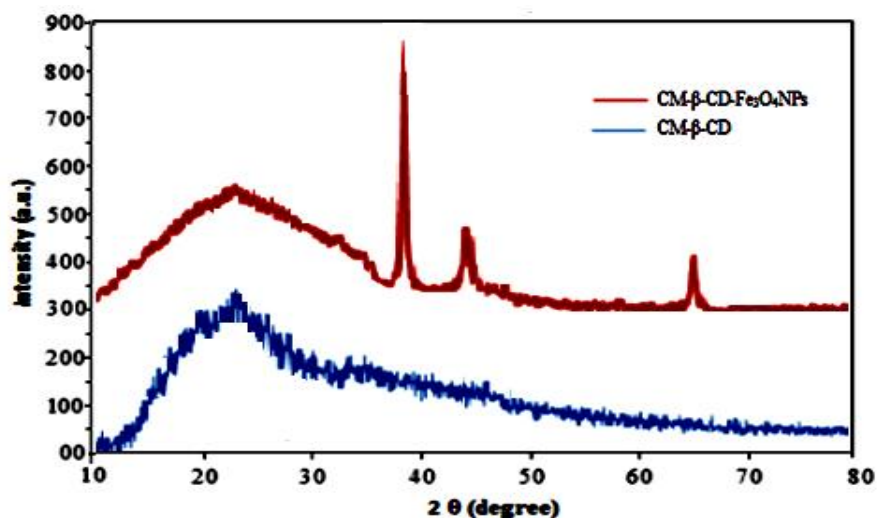
**Fig. 6.** XRD pattern of CM-β-CD and CM-β-CD-Fe$_3$O$_4$NPs.
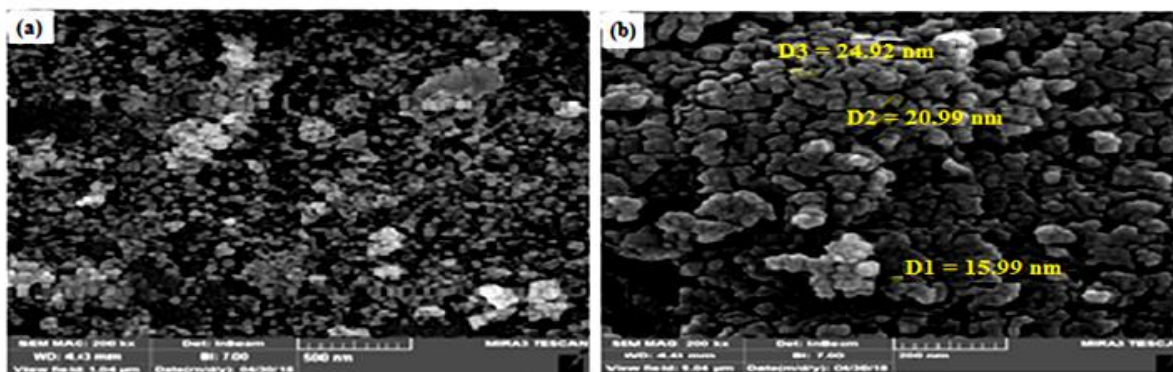


**Fig. 7.** The SEM images of the prepared CM-β-CD-Fe3O4NPs in (a) 500 nm scale (b) 200 nm scale.

The CCD avoids running unnecessary experiments while helps to investigate the synergies amongst the variables. In other words, the CCD under RSM helps to analyze the interaction between the parameters. The initial CV concentration ($X_1$), pH ($X_2$) and adsorbent dosage ($X_3$) and sonication time ($X_4$) were involved in the CCD as variables which may affect the removal percentage of CV (R%) as response. The plots of experimental removal percent versus those calculated from equations indicated a good fit. The codified values for the quadratic equations after excluding the insignificant terms are shown in Eq. (3). A detailed explanation on the CCD under RSM has been reported elsewhere [31]. The analysis of variance (ANOVA) was performed to determine the level of significance of each term (Table 4). The significance of each variable was checked from the corresponding p-value and F-value. A p-value less than 0.05 in the ANOVA table indicates the statistical significance of a variable at 95% confidence level. Desirability function (DF) was applied to investigate the optimal conditions based on Derringer's desirability function [32].

$$R\%_{CV}=95.709-2.1767X_1-1.0258X_2+0.94833X_3+6.3233X_4+2.0955X_5-1.4350X_1X_2+1.3388X_1X_3+2.9638X_1X_4-1.1638X_1X_5+0.69000X_2X_3+1.0650X_2X_4-1.3900X_2X_5-1.6612X_3X_4+1.4612X_3X_5-1.9138X_4X_5+0.66726X_1{}^2+0.91726X_2{}^2-0.020244X_3{}^2-2.8327X_4{}^2-0.41595X_5{}^2 \quad (3)$$

From ANOVA for the R% $_{CV}$, the P-values for the lack of fits corresponding to CV dye were obtained to be 0.177 which prove the applicability of the predictive models. For both models, the $R^2$ adjusted were close to 1 confirming the goodness of the fit. From Eq. (3), it is seen that the pH and its interaction with CV dye concentrations are significant which negatively affect %$R_{CV}$. Another significant variable that positively affects R%$_{CV}$ is amount of adsorbent.

## 3.3. Response Surface Plots
The 3D RSM surfaces corresponding to %$R_{CV}$ were depicted and considered to optimize the significant factors and to give useful information about the possible interaction of variables. As also seen from Fig. 8, that the dye removal percentage changes versus the adsorbent dosage [33]. The positive increase in the dye removal percentage with increase in adsorbent mass

is seen. Significant diminish in removal percentage at lower amount of CM-β-CD-Fe$_3$O$_4$NPs is attribute to higher ratio of dye molecules to the vacant sites of the adsorbent. The maximum CV dye deletion of 100%, the optimum conditions were as follows: pH of 6.0, ultrasound time of 5 min, adsorbent mass of (0.025g) and initial CV dye equal to 10.0 mgL$^{-1}$ for Crystal Violet. Additionally, to examine the optimum conditions experimentally, eleven experiments under the same conditions at 25$^0$C were conducted. Based on the great conformity between the experimental and prediction data, it was confirmed that the central composite design could be utilized successfully for the evaluation and optimization of the influences of the adsorption independent variables on the removal efficiency of CV dye from aqueous media with the help of CM-β-CD-Fe$_3$O$_4$NPs.

**Table 4.** Analysis of variance (ANOVA) for R% of CV.

| Source of variation | Df | Sum of square | Mean square | F-value | P-value |
|---|---|---|---|---|---|
| | | | CV | | |
| Model | 14 | 977.95 | 48.8980 | 8.4833 | 0.000412 |
| $X_1$ | 1 | 18.691 | 18.6910 | 3.2428 | 0.099187 |
| $X_2$ | 1 | 42.987 | 42.9870 | 7.4579 | 0.019546 |
| $X_3$ | 1 | 1.0753 | 1.0753 | 0.18655 | 0.67415 |
| $X_4$ | 1 | 515.97 | 515.9700 | 89.5160 | < 0.0001 |
| $X_1X_2$ | 1 | 49.421 | 49.4210 | 8.5741 | 0.013736 |
| $X_1X_3$ | 1 | 1.809 | 1.8090 | 0.31385 | 0.58655 |
| $X_1X_4$ | 1 | 17.808 | 17.8080 | 3.0896 | 0.10655 |
| $X_2X_3$ | 1 | 25.806 | 25.8060 | 4.4772 | 0.057977 |
| $X_2X_4$ | 1 | 48.372 | 48.3720 | 8.3921 | 0.014525 |
| $X_3X_4$ | 1 | 4.5369 | 4.5369 | 0.78711 | 0.39396 |
| $X_1^2$ | 1 | 26.291 | 26.2910 | 4.5613 | 0.056021 |
| $X_2^2$ | 1 | 26.291 | 26.2910 | 4.5613 | 0.056021 |
| $X_3^2$ | 1 | 1.2151 | 1.2151 | 0.21081 | 0.65508 |
| $X_4^2$ | 1 | 84.299 | 84.2990 | 14.6250 | 0.002822 |
| Residual | 11 | 63.404 | 5.7640 | | |
| Lack of Fit | 5 | 41.28 | 8.2561 | 2.2391 | 0.17741 |
| Pure Error | 6 | 22.123 | 3.6872 | | 0.000412 |
| Cor Total | 31 | 1041.4 | | | 0.099187 |

### 3.4. Optimization of CCD by DF for Extraction Procedure

The profile for desirable option with predicted values in the STATISTICA 10.0 software was used for the optimization of the process (Fig. 9). The desirability in the range of 0.0 (undesirable) to 1.0 (very desirable) was used to obtain a global function (D) that is the base of optimization. The CCD design matrix results were obtained as maximum (100 %) and minimum (71.9%) for CV dye. According to these values, DF settings for either of dependent variables of removal percentages were depicted on the right hand side of (Fig. 9). Desirability of 1.0 was assigned for maximum removal (99.5%) for CV dye.

### 3.5. Adsorption isotherms

The adsorbate molecules division among the solid and liquid phases in equilibrium is designated based on the isotherms of adsorption. Adsorption of CV dye onto CM-β-CD-Fe$_3$O$_4$NPs was modeled based on three adsorption isotherms of Freundlich, Langmuir, and Temkin isotherms [34].

A detailed description of adsorption isotherm at equilibrium state is possible based on the mathematical relevance between the ($q_e$) as mg/g and non-adsorbed quantity of dyes ($C_e$) as mg/L at the determined temperature. For the accurate study of adsorption isotherms, the Langmuir, Freundlich, and Temkin models were employed in Table 5. Based on the Langmuir model, at homogeneous surfaces, there is no interaction between the adsorbed molecules and the adsorption process. The following equation presents the Langmuir model [35]:

$$q_e = \frac{bq_m C_e}{1 + bC_e} \qquad (4)$$

In the above equation $C_e$, $q_e$, $q_m$ is equilibrium concentration (mg/L), adsorption capacity (mg/g), and the maximum of adsorption capacity (mg/g). The Langmuir model proved to be the best because it provides a strong correlation in all masses of adsorbent. Increasing the amount of adsorbent caused a considerable increase in the adsorbed dyes amounts. In Table 5, calculation of $K_F$ and adsorption capacity in the Freundlich model [36] was performed from the interception and slope of the linear plot of the following equation:

$$Ln(q_e) = Ln(K_F) + \frac{1}{n} Ln(C_e) \qquad (5)$$

The isotherm model of Temkin was employed to evaluate adsorption heat and interaction between adsorbent and adsorbate base on the following equation:

$$q_e = \frac{RT}{B_T} Ln(K_T) + \frac{RT}{B_T} Ln(C_e) \qquad (6)$$

In this model as mentioned above, $B_T$ (J/mol) and $K_T$ (L/mg) are Temkin constants. R and T are the universal gas constant (8.314 J/mol. K) and absolute temperature (K), respectively [37, 38].

(a)

(b)

(c)

(d)
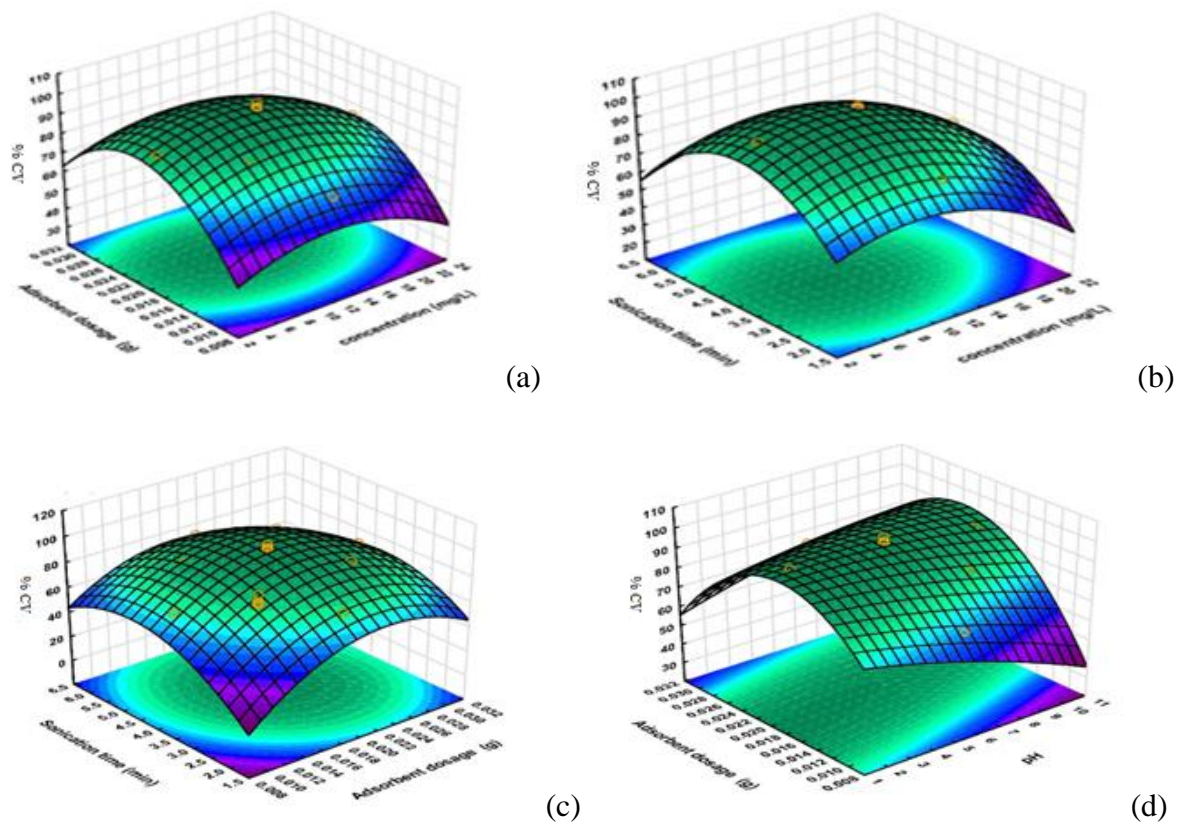
**Fig. 8.** Response surfaces for the dyes removal: (a) adsorbent dosage - initial CV concentration (b) contact time, initial CV concentration (c) contact time - adsorbent dosage (d) adsorbent dosage - pH
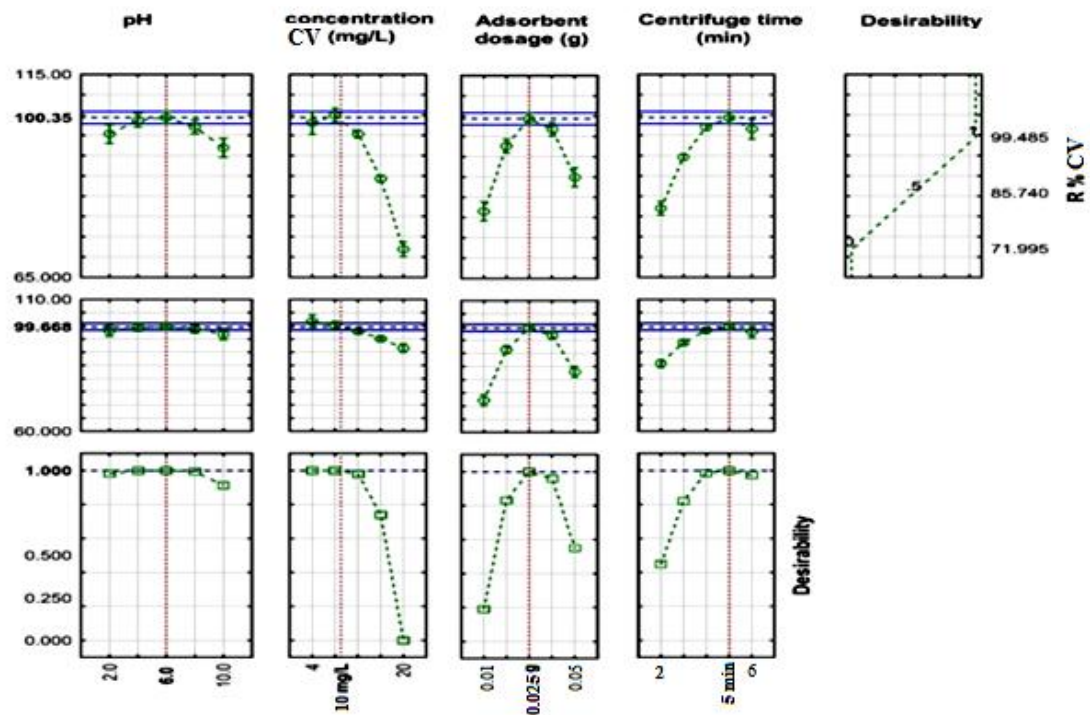


**Fig. 9.** Profiles for predicated values and esirability function for removal percentage of CV dye line indicates current values after optimization.

**Table 5.** Various isotherm constants and their correlation coefficients were calculated for the adsorption of (CV) dye onto CM-β-CD-Fe$_3$O$_4$NPs.

| Isotherm | parameters | %R$_{CV}$ |
|---|---|---|
| Langmuir | q$_m$ (mg g$^{-1}$) | 100.0 |
| | K$_L$ (L mg$^{-1}$) | 0.487 |
| | R$^2$ | 0.9898 |
| Freundlich | 1/n | 0.55 |
| | K$_F$ (mg)$^{1-n}$L$^n$g$^{-1}$ | 4.09 |
| | R$^2$ | 0.9829 |
| Temkin | B$_T$ (J mol$^{-1}$) | 14.15 |
| | K$_T$ (L mg$^{-1}$) | 6.855 |
| | R$^2$ | 0.9634 |

### 3.6. The adsorption kinetics survey

Adsorption of a solute by a solid in an aqueous solution through complex stages [38, 39], is strongly influenced by several parameters related to the state of the solid (generally with the very heterogeneous reactive surface) and to physic-chemical conditions under which the adsorption occurred. The rate of dyes adsorption onto adsorbent was fitted to traditional models like, pseudo-first and pseudo- second-models. The Lagergren pseudo-first-order model scribed the adsorption kinetic data. The Lagergren is commonly expressed as follows:

$$\frac{dq_t}{dt} = k_1(q_e - q_t) \qquad (7)$$

Where $q_e$ and $q_t$(mg/g) are the adsorption capacities at equilibrium and at time t, respectively. $k_1$ is the rate constant of the pseudo-first-order adsorption(L/min). The log (q$_e$−q$_t$) versus t was plotted and the values of **k$_1$** and **q$_e$** were determined by using the slope and intercept of the line, respectively [40].

$$\text{Log} (q_e - q_t) = \text{Log} (q_t) - \frac{k_1}{2.303}t \qquad (8)$$

The fact that the intercept is not equal to **q$_e$** imply that there action is unlikely to follow the first-order. The relationship between initial solute concentration and rate of adsorption is linear when pore diffusion limits the adsorption process. Therefore, it is necessary to fit experimental data to another model (Table 6) such as pseudo-second-order model [41], based on the following equation:

$$\frac{dq_t}{dt} = k_2(q_e - q_t)^2 \qquad (9)$$

Eq. (9) is integrated over the interval 0 to t for t and 0 to $q_t$ for **q$_t$**, to give:

$$\frac{t}{q_t} = \frac{1}{k_2q_e^2} + \frac{t}{q_e} \qquad (10)$$

As mentioned above, the plot of log (**q$_e$**−**q$_t$**) versus t does not show good results for the entire sorption period, while the plot of **t/q$_t$** versus t shows a straight line. The values of k$_2$ and equilibrium adsorption capacity (**q$_e$**) were calculated from the intercept and slope of the plot of t/q versus t (Table 6). The calculated q$_e$ values at different working conditions like various initial dyes concentrations and/or adsorbent masses were close to the experimental data and higher R$^2$ values corresponding to this model confirm its more suitability for the explanation of experimental data [40, 41]. This indicates that the pseudo-second-order kinetic model applies better for the adsorption of the CV dye system for the entire sorption period. The kinetic data from pseudo-first and pseudo-second-order adsorption kinetic models are given in Table 6. The linear plots of **t/q$_t$** versus t indicated a good agreement between the experimental and calculated **q$_e$**values for different initial dye concentrations. Furthermore, the correlation coefficients of the pseudo-

second-order kinetic model ($R^2$=0.9995) were greater than that of the pseudo-first-order model ($R^2$= 0.9894) for CV dye. As a result, the adsorption fits the pseudo-second-order better than the pseudo-first-order kinetic model.

### 3.7. Adsorption thermodynamics

For the adsorption processes, 3 thermodynamic parameters of 1-Gibbs free energy change ($\Delta G°$), 2- enthalpy change ($\Delta H°$) and 3- entropy change $\Delta S°$ were considered. Their computation becomes possible through utilizing the ensuing equations [43]:

$$\Delta G° = - RT \ln K_{ad} \tag{11}$$

$$\ln K_{ad} = \frac{- \Delta H°}{RT} + \frac{\Delta S°}{R} \tag{12}$$

From a plot of $\ln K_{ad}$ against $1/T$, by considering the slope of this graph $\Delta G°$ can be acquired. In Table 7, the summary of the thermodynamic parameter outcomes for the adsorption of CV dye onto CM-β-CD-Fe$_3$O$_4$NPs at diverse temperatures is demonstrated. The estimation of $\Delta G°$ values became possible via employing the equation adsorption of CV dye. As can be seen in (Table 7), with any increase in the temperature from 288.0 to 338.0 K, a steep reduction in the CM-β-CD-Fe$_3$O$_4$NPs adsorbent was observed which confirms the exothermicity nature of the process. The thermodynamic parameters such as free energy ($\Delta G^0$), enthalpy ($\Delta H^0$), and entropy ($\Delta S^0$) of adsorption. The value of ($\Delta G°$, $\Delta H°$, and $\Delta S°$) confirmed the sorption process was endothermic reflects the affinity of CM-β-CD-Fe$_3$O$_4$NPs for removing CV dye process requires heat [44].

**Table 6.** Various Kinetic constants and their correlation coefficients were calculated for the adsorption of (CV) dye onto CM-β-CD-Fe$_3$O$_4$NPs.

| Models | parameters | %$R_{CV}$ |
|---|---|---|
| pseudo-First-order kinetic | $k_1$(min$^{-1}$) | 0.987 |
| | $q_e$ (mg g$^{-1}$) | 17.92 |
| | $R^2$ | 0.9894 |
| pseudo-Second-order kinetic | $k_2$ (min$^{-1}$) | 0.154 |
| | $q_e$ (mg g$^{-1}$) | 15.56 |
| | $R^2$ | 0.9995 |
| Intraparticle diffusion | $K_d$ (mg g$^{-1}$ min$^{-1/2}$) | 8.050 |
| | C (mg g$^{-1}$) | 77.33 |
| | $R^2$ | 0.9859 |
| $q_e$(exp) (mg g$^{-1}$) | | 102.5 |

**Table 7.** The thermodynamic parameters for the adsorption of CV dye onto CM-β-CD-Fe$_3$O$_4$NPs adsorbent.

| Dye (mg/L) | T ($^O$K) | $K_c$ | value of $\Delta G°$(kJ/mol) | value of $\Delta H°$(kJ/mol) | value of $\Delta S°$ (kJ/mol K) |
|---|---|---|---|---|---|
| Crystal Violet (CV) (10 mgL$^{-1}$) | 288 | -47.66 | 95.58 | -29.24 | -131.49 |
| | 308 | -57.4 | -103.73 | | |
| | 318 | -96.33 | -120.85 | | |
| | 328 | -145.0 | -135.77 | | |
| | 338 | -291.0 | -159.40 | | |

## 3.8. Recycling of the Adsorbent

The ability of recovering and reusing of the adsorbent was tested in several steps of adsorption and the desorption process were done [45]. The results are shown in Fig. 10. As shown in the figure 98.0% of CV dye was desorbed in the first run and after 6 runs, there were slight changes in CV dye desorption. So, it was concluded that the desired removal of 98% can be achieved after 6 runs.

## 3.9. Comparison of the CV dye adsorption onto other adsorbents

A comparison of the maximum adsorption capacities of different adsorbents for the removal of CV dye was also reported in Table 8. The type and density of active sites in adsorbents those are responsible for the adsorption of CV dye from the solution result in the variation in $q_{max}$ values. The outcomes of the table clearly show that the sorption capacity of the utilized sorbent in the current study is significantly high. In general, morphology, particle size and distribution, and surface structure of this sorbent were effective in its successful outcomes.
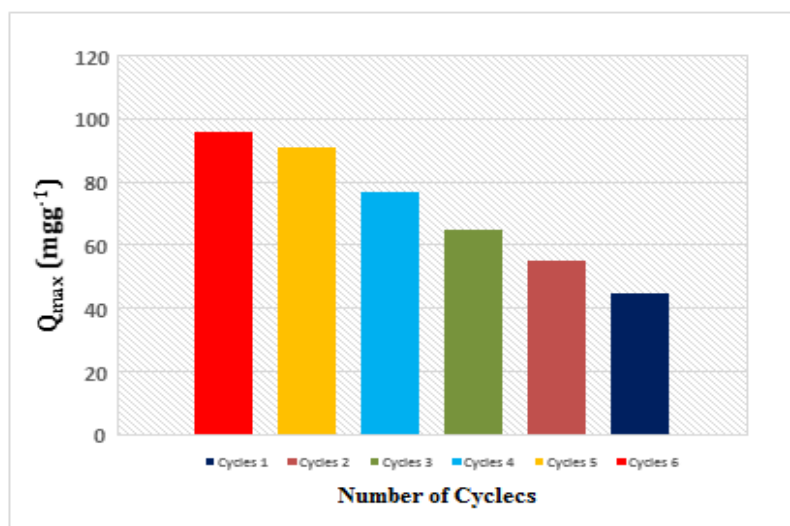


**Fig. 10.** Desorption of CV dye from CM-β-CD-Fe$_3$O$_4$NPs. [C$_0$= 10.0 mgL$^{-1}$, pH = 6.0, dose = 0.025 g, t$_c$ = 5.0 min, T=25 °C].

**Table 8.** The juxtaposition of the adsorption capacities of different adsorbents for the adsorption of CV dye onto sorbent.

| Dye | Adsorbent | Dosage sorbent | pH | Time | Adsorption capacity | References |
|---|---|---|---|---|---|---|
| Crystal Violet (CV) | potato peels | 0.500 g | 6.0 | 20 min | 55.50 mgg$^{-1}$ | [6] |
| Crystal Violet (CV) | powder of Ceriporia lacerata | 2.500 g | 5.5 | 45 min | 50.00 mgg$^{-1}$ | [7] |
| Crystal Violet (CV) | flow bone char | 1.000 g | 6.0 | 74 min | 20.42 mg g$^{-1}$ | [8] |
| Crystal Violet (CV) | Onion Skins | 0.010 g | 2.0 | 150 min | 51.30 mg g$^{-1}$ | [9] |
| Crystal Violet (CV) | Activated Carbon | 0.050 g | 6.0 | 15 min | 89.92 mgg$^{-1}$ | [20] |
| Crystal Violet (CV) | brown algae Padina sanctae-crucis | 0.250 g | 2.0 | 10 min | 10.02 mgg$^{-1}$ | [37] |
| Crystal Violet (CV) | CM-β-CD-Fe$_3$O$_4$NPs | 0.025 g | 6.0 | 5 min | 100.00 mgg$^{-1}$ | Present study |

## 4. CONCLUSION

A thorough investigation was performed on the effectiveness of synthesized CM-β-CD-Fe$_3$O$_4$NPs as an adsorbent for the removal of CV dye from aqueous solutions has been investigated. The experiments were designed by response surface methodology and a quadratic model was used for the prediction of the variables. The influence of process variables CV dye concentration, pH, adsorbent mass, and contact time on the adsorption of CV dye was investigated by central composite design (CCD) of RSM. The adsorption of CV dye onto CM-β-CD-Fe$_3$O$_4$NPs was found to be 99.2% at pH: 6.0, CV dye concentration: 10.0 mg L$^{-1}$, adsorbent mass: 0.025, and sonication time: 5.0 min. At optimum adsorption conditions, the experimental removal efficiency of CM-β-CD-Fe$_3$O$_4$NPs reached (R$^2$= 0.97-0.99) for CV dye. Different isotherm models (Langmuir, Freundlich, and Temkin isotherms) have been examined for the adsorption process but it became apparent that the Langmuir model could successfully describe the equilibrium data. The maximum (q$_{max}$) value of 100.0 mgg$^{-1}$ for CV dye. The process kinetics was found to be effectually fitted to the pseudo-second-order kinetic model. In addition, the possibility of recycling the adsorbent was well proved by desorption studies. Based on the results from the linear regression-based analysis, it was revealed that the derived empirical models represented a passable prediction of performance onto CM-β-CD-Fe$_3$O$_4$NPs with significant determination coefficients CV dye (R$^2$= 0.999). Additionally, at the temperatures under investigation, spontaneous adsorption of CV dye was reported. Also, the exothermicity of the sorption process was confirmed by the negative values of ($\Delta G^o$, $\Delta H^o$, and $\Delta S^o$). The study aimed at developing low-cost, highly available, and powerful CV dye adsorbents from natural wastes for the replacement of existing commercial adsorbents. CM-β-CD-Fe$_3$O$_4$NPs in comparison with other adsorbents show a high adsorption capacity for CV dye deletion from an aqueous medium.

## CONFLICT OF INTEREST

The authors declare that they have no conflict of interest related to the publication of this article.

## REFERENCES

[1] G. H. Vatankhah, A. Kohmareh, Enhanced removal of Bismark Brown (BB) dye from aqueous solutions using activated carbon from raw Ziziphusspina-christi (ZSAC) Equilibrium, thermodynamic and kinetics. J. Phys. Theore. Chem. 14(3) (2018) 237-249.

[2] Z. Zubair, I. Ihsanullah, N. Jarrah, A. Khalid, M.S. Manzar, T.S. Kazeem, M.A. Al- Harthi, Starch-NiFe-layered double hydroxide composites: efficient removal of methyl orange from aqueous phase, J. Molecular Liquids. 249 (2018) 254–264.

[3] A.H. Jawad, A.S. Abdulhameed, Acid-factionalized biomass material for methylene blue dye removal: a comprehensive adsorption and mechanism study, J. Taibah, Univ. Sci. 14 (2020) 305-313.

[4] I. Ihsanullah, A. Jamal, M. Ilyas, M. Zubair, G. Khan, M.A. Atieh, Bioremediation of dyes: Current status and prospects. J. Water Proces Eng. 38 (2020) 101680.

[5] V. Kumar, P. Saharan, A.K. Sharma, A. Umar, I. Kaushal, Y. Al-Hadeethi, B.

Rashad, A. Mittal, Silver doped manganese oxide-carbon nanotube nanocomposite for enhanced dye-sequestration: Isotherm studies and RSM modelling approach, J. Ceramics International. 46 (2020) 10309-10319.

[6] S. Lairini, K. El Mahtal, Y. Miyah, K. Tanji, S. Guissi, S. Boumchita, F. Zerrouq, The adsorption of Crystal violet from aqueous solution by using potato peels (Solanumtuberosum): equilibrium and kinetic studies, J. Mater. Environ. Sci. 8 (2017) 3252-3261.

[7] M. Zamouche,A. Habib,K. Saaidia, M. B. Lehocine, Batch mode for adsorption of Crystal Violet by cedar cone forest waste, SN Appl. Sci. 2 (2020) 198-212.

[8] M. Alexandra Pires Cruz, L.C.M. Guimarães, E.F. da Costa Júnior, S.D. Ferreira Rocha, P. da Luz Mesquita, Adsorption of crystal violet from aqueous solution in continuous flow system using bone char, Chem. Eng. Communications. 207(3) (2020) 372-381.

[9] F.N. Ghazi,I.H. Dakhil,A.H. Ali,A.H. Taha, MethyleneViolet Dye Adsorption Using Onion Skins: Kinetics and Isotherm Studies, Mater. Sci. Eng. 1090 (2021) 12047.

[10] F. Marahel, B. MombeniGoodajdar, L. Niknam, M. Faridnia, E. Pournamdari, S. MohammadDoost, Ultrasonic Assisted Adsorption of Methylene Blue Dye and Neural Network Model for Adsorption of Methylene Blue Dye by Synthesized Mn-doped PbS nanoparticles. Int. J. Environ. Anal. Chem. (2021).

[11] A. Reghioua, D. Barkat, A.H. Jawad, A.S. Abdulhameed, A.A. Al-Kahtani, Z.A. ALOthman, Parametric optimization by Box–Behnken design for synthesis of magnetic chitosan-benzil/ZnO/Fe₃O₄nanocomposite and textile dye removal, J. Environ. Chem. Eng. 9 (2021) 105166.

[12] F. Ramezani, R. Zare-Dorabei, Simultaneous ultrasonic-assisted removal of malachite green and methylene blue from aqueous solution by Zr-SBA-15, Polyhedron. 166 (2019) 153-162.

[13] M. Kiani, S. Bagheri, N. Karachi, E. AlipanahpourDil, Adsorption of purpurin dye from industrial wastewater using Mn-doped $Fe_2O_4$ nanoparticles loaded on activated carbon, Desal. Water Treat. 152 (2019) 366-378.

[14] E. AlipanahpourDil, M. Ghaedi, A. Asfaram, A.A. Bazrafshan, Ultrasound wave assisted adsorption of congo red using gold-magnetic nanocomposite loaded on activated carbon: Optimization of process parameters, Ultrasonics − Sonochemistry. 46 (2018) 99–105.

[15] A.H. Jawad, A.S. Abdulhameed, Statistical modeling of methylene blue dye adsorption by high surface area mesoporous activated carbon from bamboo chip using KOH-assisted thermal activation, Energ. Ecol. Environ. (2020).

[16] A. Reghioua, D. Barkat, A.H. Jawad, A.S. Abdulhameed, M.R. Khan, Sustaina. Synthesis of Schiff's base magnetic crosslinked chitosan-glyoxal/ZnO/Fe₃O₄ nanoparticles for enhanced adsorption of organic dye: Modeling and mechanism study, Sustaina. Chem. Pharmac. 20 (2021) 100379.

[17] S. Zeinali, M. Abdollahi, S. Sabbaghi, Carboxymethyl-β-cyclodextrin Modified Magnetic Nanoparticles for Effective Removal of Arsenic from Drinking Water: Synthesis and Adsorption Studies, J. Water Environ. Nanotechnol., 1(2): 104-115, Autumn 2016.

[18] J. Zhu, P. Wang, M. Lu, β-Cyclodextrin coated Fe₃O₄ nanoparticles: a simple preparation and application for selective

oxidation of alcohols in water, J. Braz. Chem. Soc. 24 (2013) 171-176.

[19] A. A. Ghazali, F. Marahel, B. MombeniGoodajdar, SynthesizedCM-β-CD-Fe$_3$O$_4$NPs: As an Environmental Friendly and Effective Adsorbent for Elimination of Boron from Aqueous Solutions Int. J. Environ. Anal. Chem. (2021).

[20] F. Hayeeye, M. Sattar, A. Benhawan, Optimization of Preparation Conditions and Characterization for Dialiumcochinchinensis Seed Activated Carbon, RSU. Int. Res. 4 (2020) 681-686.

[21] A.R. Parvizi, B. Bagheri,N. Karachi, L. Niknam, Preparation and characterization of Titanium dioxide nanoparticles for the Removal of Disulfine Blue and Methyl Orange: spectrophotometric detection and optimization. Orient. J. Chem. 32 (2017) 549-565.

[22] A.R. Bagheri, M. Ghaedi, S. Hajati, A.M. Ghaedi, A. Goudarzi, A. Asfaram, Random forest model for the ultrasonic-assisted removal of chrysoidine G by copper sulfide nanoparticles loaded on activated carbon; response surface methodology approach, RSC Adv. 5 (2015) 59335-59343.

[23] F. Raoufi, H. Aghaee, M. Monajjemi, Modeling of Competitive Ultrasonic Assisted Removal of the Crystal Violet and Auramine O using MWCNTs Functionalized by N-(3-nitrobenzylidene)-N' -trimethoxysilylpropyl-ethane-1,2-diamine: Equilibrium, Kinetics and Thermodynamic Study. Orient. J. Chem. 32 (2016) 1839-1858.

[24] A. Asfaram, M. Ghaedi, S. Hajati, A. Goudarzi, Synthesis of magnetic gamma-Fe$_2$O$_3$-based nanomaterial for ultrasonic assisted dyes adsorption: Modeling and optimization, UltrasonSonochem. 32 (2016) 418-431.

[25] H.S. Ghazi Mokri, N. Modirshahla, M.A. Behnajady, B. Vahid, Adsorption of C.I. Acid Red 97 dye from aqueous solution onto walnut shell: kinetics, thermodynamics parameters, isotherms. Int. J. Environ. Sci. Technol. 12 (2015) 1401–1408.

[26] G. Mamba, X.Y. Mbianda, P.P. Govender, B.B. Mamba,R.W. Krause, Application of Multiwalled Carbon Nanotube-Cyclodextrin Polymers in the Removal of Heavy Metals from Water, Journal of Applied Sciences. 10 (2010) 940-949.

[27] S. Bagheri, H. Aghaei, M. Ghaedi, M. Monajjemi, K. Zare, Novel Au–Fe$_3$O$_4$ NPs Loaded on Activated Carbon as a Green and High Efficient Adsorbent for Removal of Dyes from Aqueous Solutions: Application of Ultrasound Wave and Optimization, Eurasian Journal of Analytical Chemistry. 13(3) (2018) 1-10.

[28] S. Kaur, A. Gaur, Structural and Photoluminescence Study of Iron Oxide Nanoparticles, Advanced Science Letters. 20 (2014) 1707-1709.

[29] A.Z.M. Badruddoza, S.S.H. Goh, K. Hidajat, M.S. Uddin, Synthesis of Carboxymethyl-β-Cyclodextrin Conjugated Magnetic Nano-Adsorbent for Removal of Methylene Blue. Colloids and Surfaces A: Physicochemical and Engineering Aspects, 367 (2010) 85-95.

[30] M. Moradi, M. Hosseini, F. Marahel, A. Shameli, Removal of reactive green KE-4BD and Congo red dyes in textile effluent by natural clinoptilolite particles on a biosorbent as a cheap and efficient adsorbent: experimental design and optimization, Int. J. Environ. Anal. Chem. (2021).

[31] H.Z. Khafri, M. Ghaedi, A. Asfaram, M. Safarpoor, Synthesis and characterization of ZnS: Ni-NPs loaded on AC derived from apple tree wood and their applicability for the ultrasound

assisted comparative adsorption of cationic dyes based on the experimental design, Ultrason. Sonochem. 38 (2017) 371.

[32] B. Mombeni Goodajdar, F. Marahel, L. Niknam, E. Pournamdari, E. Mousavi, Ultrasonic Assisted and Neural Network Model for Adsorption ofofhumic acid (HAs) by SynthesizedCM-β-CD-Fe$_3$O$_4$NPs from Aqueous Solutions, Int. J. Environ. Anal. Chem. (2021).

[33] M. Pargari, F. Marahel, B. MombiniGodajdar, Ultrasonic Assisted Adsorption of Propyl Paraben on Uultrasonically Synthesized TiO$_2$nano particles loaded on activated carbon: Optimization, kinetic and equilibrium studies, Desal. Water Treat. 212 (2021) 164-172.

[34] S. Hajati, M. Ghaedi, B. Barazesh, F. Karimi, R. Sahraei, A. Daneshfar, A. Asghari, Application of high order derivative spectrophotometry to resolve the spectra overlap between BG and MB for the simultaneous determination of them: ruthenium nanoparticle loaded activated carbon as adsorbent, J. Ind. Eng. Chem. 20 (2014) 2421–2427.

[35] Y. Yang, Y. Xie, L. Pang, M. Li, X. Song, J. Wen and H. Zhao, Preparation of reduced graphene oxide/poly(acrylamide) nanocomposite and its adsorption of Pb$^{2+}$ and methylene blue. Langmuir. 29 (2013) 10727.

[36] M. Kiani, S. Bagheri, A. Khalaji, N. Karachi, Ultrasonic supported deletion of Rhodamine B on ultrasonically synthesized zinc hydroxide nanoparticles on activated carbon concocted from wood of cherry tree: experimental design methodology and artificial neural network, Desal. Water Treat. 226 (2021) 147-156.

[37] R. Mahini, H. Esmaeili, R. Foroutan, Adsorption of methyl violet from aqueous solution using brown algae Padinasanctae-crucis. Turk. J. Biochem. 24 (2018) 1-12.

[38] A. Azari, R. Nabizadeh, S. Nasseri, A.H. Mahvi, A.R. Mesdaghinia, Comprehensive systematic review and meta-analysis of dyes adsorption by carbon-based adsorbent materials: Classification and analysis of last decade studies, Chemosphere. 250 (2020) 126238.

[39] M. Hubbe, S. Azizian, S. Douven, Implications of Apparent Pseudo-Secound-Order Adsorption Kinetics onto Cellulosic Materials: A Review, Bio Resources. 14(3) (2019) 7582-7626.

[40] T. Taher, D. Rohendi, R. Mohadi, A. Lesbani, Congo red dye removal from aqueous solution by acid-activated bentonite from sarolangun: kinetic, equilibrium, and thermodynamic studies, Arab. J. Basic Appl. Sci. 26 (2019) 125-136.

[41] V. M. Muinde, J. M. Onyari, B. Wamalwa, J. N. Wabomba, Adsorption of malachite green dye from aqueous solutions using mesoporous chitosan–zinc oxide composite material, Environmental Chemistry and Ecotoxicology, Volume 2, 2020, Pages 115-125

[42] N.N. AbdMalek, A.H. Jawad, A.S. Abdulhameed, K. Ismail, B.H. Hameed, New magnetic Schiff's base-chitosan-glyoxal/fly ash/Fe$_3$O$_4$ biocomposite for the removal of anionic azo dye: An optimized process, Int. J. Biolog. Macromolecules. 146 (2020) 530–539.

[43] Sh. Bouroumand, F. Marahel, F. Khazali, Removal of Yellow HE4G dye from Aqueous Solutions Using synthesized Mn-doped PbS (PbS:Mn) nanoparticles, Desal. Water Treat. 223 (2021) 388-392.

[44] A.H. Jawad, A.S. Abdulhameed, Statistical modeling of methylene blue dye adsorption by high surface area mesoporous activated carbon from

bamboo chip using KOH-assisted thermal activation, Energ. Ecol. Environ. (2020).

[45] E. Mousavi, A. Geramizadegan, Adsorption of Benzyl Paraben Dye from Aqueous Solutions Using synthesized Mn-doped PbS (PbS:Mn) nanoparticles, J. Phys. Theore. Chem. 17(3, 4), (2020) 123-143.

# حذف رنگ بنفش کریستال با استفاده از جاذب سنتزی سیکلودکسترین اصلاح شده با نانو ذرات اکسید آهن و به کمک امواج فراصوت؛ با متدلوژی طراحی تجربی

علی عمانی زیارتی[1] و غلامحسین وطن خواه[2*]

1- دانشگاه آزاد اسلامی واحد دشتستان، گروه مهندسی شیمی، دشتستان، ایران.

2- دانشگاه آزاد اسلامی واحد بوشهر، گروه مهندسی شیمی، بوشهر، ایران.

## چکیده

در این پژوهش، کاربرد جاذب سیکلو دکسترین/نانو ذرات اکسید آهن سنتز شده به عنوان یک جاذب جدید برای حذف رنگ بنفش کریستال از محیط های آبی مورد بررسی قرار گرفت. این مقاله بر توسعه یک روش موثر برای به دست آوردن شرایط بهینه حذف با کمک امواج فراصوت برای حذف حداکثر رنگ بنفش کریستال بر روی CM-β-CD-Fe3O4NPs در یک محلول آبی با استفاده از روش سطح پاسخ (RSM) تمرکز دارد. این جاذب جدید با تکنیک‌های مختلف مانند FT-IR ، XRD و SEM مشخصه یابی و ارزیابی گردید. تأثیر متغیرهایی مانند غلظت اولیه رنگ ($X_1$)، pH ($X_2$)، دوز جاذب ($X_3$) و زمان فراصوت ($X_4$) با طراحی مرکب مرکزی (CCD) تحت روش سطح پاسخ مورد بررسی قرار گرفت. این فرآیند به صورت تجربی مدل-سازی شد تا متغیرهای مهم و فعل و انفعالات احتمالی آنها آشکار شود. شرایط بهینه سازی برای زمان تابش امواج فراصوت، pH ، مقدار جاذب وغلظت رنگ به ترتیب، 10 میلی‌گرم بر لیتر، 6، 5 دقیقه و 0/025 گرم تعیین شد. در نهایت، نشان داده شد که حذف رنگ بنفش کریستالی توسط جاذب در pH برابر با 6 اتفاق افتاد. به وضوح ثابت شد که جذب رنگ مورد مطالعه با معادله سینتیکی شبه درجه دوم مطابقت دارد و همدمای لانگمویر داده های تعادل را توضیح می‌دهد. حداکثر ظرفیت تک لایه جذب توسط جاذب ($q_{max}$) برای رنگ مورد مطالعه در شرایط بهینه 100 میلی‌گرم بر گرم بدست آمد. گرمازا بودن این فرآیند با مقدار منفی ($\Delta G°$، $\Delta H°$ و $\Delta S°$) ثابت شد که نشان از میل جاذب سنتز شده CM-β-CD-Fe3O4NPs برای حذف رنگ بنفش کریستال دارد.

**کلمات کلیدی**: جذب، رنگ بنفش کریستال، جاذب سیکلو دکسترین/نانوذرات اکسید آهن، طراحی مرکب مرکزی، روش سطح پاسخ.

* مسئول مکاتبات: gh.vatankhah@iau.ac.ir